It's not hot air: Using GOES-16 infrared window bands to diagnose adjacent summertime air masses

Jordan J. Gerth, corresponding author, Cooperative Institute for Meteorological Satellite Studies, Space Science and Engineering Centre, University of Wisconsin-Madison
1225 W. Dayton St.
Madison, Wisconsin 53706
jordan.gerth@ssec.wisc.edu

Abstract

The first in the next-generation series of United States Geostationary Operational Environmental Satellites (GOES), GOES-16, is providing improved quality satellite imagery of atmospheric phenomena and land features over the Americas and the Atlantic Ocean, benefitting scientists and operational meteorologists. A frontal passage separating distinct air masses for a typical warm season case over the Upper Midwest on 30 August 2017 is examined in a discussion on the value of GOES-16 infrared window band imagery. The "split window" difference between the 10.3-μm and 12.3-μm longwave infrared bands, a traditional approach to visually characterizing low-level water vapour in cloud-free scenes, is compared to the 3.9-μm shortwave infrared window band for identifying two distinct air masses. Surface station temperatures and dew points confirm modest moisture pooling ahead of the southward-moving front. These window bands are not new to the geostationary orbit, but with GOES-16, they are available at higher bit depths and at better spatial, spectral, and temporal resolutions. This makes identifying and analysing fronts and air masses more apparent compared to legacy imagery, particularly during the day if properly enhanced. While a hindrance to quantitative approaches, solar contamination in the 3.9-μm band can be beneficial to analysts visually performing this task.

Keywords

Remote sensing, satellite observations

GOES-R, ABI, land surface temperature, solar reflection, split window difference

Body Text

(1) Introduction

The Geostationary Operational Environmental Satellite R-Series (GOES-R) Advanced Baseline Imager (ABI) on the first satellite in the latest series, GOES-16, is providing imagery at improved spatial, spectral, and temporal resolution to assist in monitoring the evolving atmosphere (Schmit et al., 2005), routinely scanning the Americas, particularly the contiguous United States. GOES-16 and subsequent satellites in the GOES-R series have sixteen spectral bands in the visible, near-infrared, and infrared portions of the electromagnetic spectrum, are capable of capturing imagery every 30 seconds in configurable interest areas, and provide infrared band imagery at a spatial resolution of 2 km (Schmit et al., 2005). GOES-16 use in the United States National Weather Service began in 2016, triggering a training effort and spawning research to redesign operational workflows around the new geostationary satellite capabilities and their unique applications. Early evaluation of the imagery has found subtle but important distinguishing characteristics between legacy and new generation GOES.

This study uses GOES-16 and -13, at a subpoint of 89.5° W and 75.0° W, respectively, to visually examine a frontal passage in the Upper Midwest on 30 August 2017, where a seasonally cooler and drier air mass was advecting out of Canada toward a warmer and moister summertime air mass over the Upper Mississippi Valley. Convergence along the front, confirmed with surface observations, supports convection that is evident in the imagery. In adjacent clear sky, the 3.9-µm shortwave infrared band, 10.3-µm "clean" longwave window band, and 12.3-µm "dirty" longwave infrared band on the GOES-16 ABI are compared in a discussion of their use to distinguish between two air masses. The National Environmental Satellite, Data, and Information Service (NESDIS) deemed the preliminary, non-operational GOES-16 imagery used in this article of provisional maturity, making it suitable for applications that involve visual interpretation such as this. Simulated imagery is used to confirm the quality of the imagery and suitability of the application for operational meteorologists.

These bands also existed on previous geostationary satellite imagers, though the 12.3-μm band was replaced with the 13.3-μm band for the imagers on GOES-13 through -15. Beyond improvements to the spatial, spectral, and temporal resolution, the imagery from the ABI is collected and distributed at a greater bit depth and the nine ABI longwave infrared bands have a better noise equivalent differential temperature (NEdT) than the legacy geostationary satellite imagers (Schmit et al., 2017). The result is higher fidelity imagery that requires proper enhancement for the analyst to qualitatively evaluate. The proper enhancement is particularly necessary for a single band application with a substantial range between minimum and maximum brightness temperatures.

(2) Discussion

In selecting the aforementioned infrared bands for this study, the radiative characteristics of the bands for monitoring air masses, the season, the time of day, and the cloudiness of the scene away from the front were considered. While the ABI has three “water vapour” bands, those bands generally do not sense the entire depth of the troposphere, particularly in mid-latitude moist regimes, making it difficult to assess near-surface air mass properties. Therefore, they are unable to diagnose near-surface fronts, particularly in the summer.

Bands in atmospheric “windows” are largely sensitive to surface properties that evolve diurnally, but partially capture lower tropospheric properties from weak water vapour absorption.

This article focuses on three of those potential bands, the 3.9 µm, 10.3 µm, and 12.3 µm, and their differences. There are other window bands, but they are not particularly unique for assessing low-level water vapour absorption compared to those aforementioned; for example, the spectral response function for the 11.2-µm band, which operational meteorologists previously used as the sole infrared window band for analyses, is between the 10.3-µm and 12.3-µm bands. Therefore, brightness temperatures for the 11.2-µm band, which is similar to legacy infrared window bands, should be less than 10.3-µm band brightness temperatures and greater than 12.3-µm band brightness temperatures for the cloud-free scene air mass application.

(2.1) 10.3-µm and 12.3-µm bands

Brightness temperature differences between ABI window bands are small but meaningful for cloud-free scenes. Analysts conducting a cursory visual inspection of such a scene in the infrared window band at 12.3 µm independently of the 10.3-µm band may conclude there are few if any meaningful differences between them and the 3.9-µm band, especially at night. However, a band difference between the 10.3-µm and 12.3-µm bands, known as the "split window" difference (SWD), can enhance slight differences to corroborate the front seen in the 3.9-µm band and evince a low-level moisture plume (Lindsey et al., 2014). Video S1(a) reveals the presence of a low-level moisture plume for this case across southern Minnesota.

A plume of 3 °C to 7 °C differences is evident in clear sky from southern Minnesota into northern Iowa and southern Wisconsin. The brightness temperatures of the infrared window bands that are part of the SWD depend on both the land type and skin temperature (Sun, 2003). Therefore, heating and cooling of the land surfaces as part of the diurnal cycle impacts brightness temperatures of infrared window bands in cloud-free areas (an animation is available in the supplemental material for online readers). While this makes it difficult to apply as an indicator in a quantitative algorithm (Chesters et al., 1983), visual inspection can overcome this complication when a precise retrieval is unnecessary. Unlike at 3.9 μm though, incoming solar radiation does not impact the SWD directly through shortwave reflection.

In clear skies, a positive 10.3–12.3 μm difference, resulting from a greater brightness temperature at 10.3 μm than at 12.3 μm, can be an effective indicator of low-level water vapour absorbing longwave radiation, provided that temperatures decrease with height away from the surface, as they would with a well-mixed boundary layer which typically evolves at the peak of diurnal heating. Since brightness temperatures of infrared window bands depend not only on the surface and concentration of water vapour (i.e., specific humidity) above the surface, but also the temperature of the layers in which the concentrated water vapour resides, the magnitude of the SWD depends on the characteristics of the lower tropospheric profile (e.g., lapse rate) and emitting surface, and varies diurnally.

(2.2) 3.9-μm band

While both the 10.3-μm band and 12.3-μm band are longwave infrared window bands, the 12.3-μm band is "dirtier" due to slightly greater water vapour absorption and thus depicts typically lesser clear-sky brightness temperatures than corresponding scenes in the 10.3-μm band. For many summertime scenes that contain deep tropospheric moisture, the 3.9-μm band is a "cleaner" window than the 10.3-μm band, as the weighting functions in Figure S1 indicate decreased sensitivity, and thus heightened transmittance, for lower tropospheric water vapour. Despite a similar central wavelength, the spectral width of the 3.9-μm band on the ABI is narrower than the corresponding 3.9-μm band on the legacy geostationary satellites (Schmit et al., 2005). As a result, sensing predominantly the background earth surface, the ABI 3.9-μm band brightness temperatures of cloud-free scenes can be slightly greater than corresponding brightness temperatures from legacy imagers, even without considering solar illumination effects. This is due to differences in the atmospheric absorption and mean surface emissivity over the respective bands, though water vapour and other trace gas absorption in the 3.9-µm band is relatively small.

The limited effects of water vapour absorption in the ABI 3.9-µm band makes it desirable for assessing a land surface temperature gradient independent of moisture. Land surface temperatures are positively correlated with near-surface air temperatures, though difficult to quantify, particularly in clear skies and during the day (Gallo et al., 2011). The 3.9-µm band can also lessen the evidence of small, thin, and/or scattered clouds due to greater transmission of longwave radiation through such types of cloud fields (Dostalek et al., 1997) and the limited influence of cooler sub-pixel cloud on the overall pixel brightness temperature compared to an uncovered surface as a consequence of Planck's law. However, during the day, the 3.9-µm band captures reflected shortwave radiation in addition to outgoing longwave radiation. This can complicate the quantitative algorithms and visual interpretation of imagery from this band, especially if not considered.

Sunlight inflates daytime brightness temperatures, with the degree of influence depending on the reflecting feature or surface properties. Solar reflection increases many land surface brightness temperatures, with the magnitude of the impact dependent on the land type (Sun et al., 2013). Mie scattering of coarse crustal and hygroscopic aerosols in the atmosphere, at least 1 µm in size, can also increase brightness temperatures. The scattering of solar radiation in the shortwave infrared window is useful in detecting aerosols such as dust when compared to the longwave infrared window (Ackerman, 1989). During the summer, the aerosol volume distributions of coarse aerosols in the lower troposphere are higher than in other seasons over the central United States (Kim et al., 1988).

The effects of solar reflection, in addition to diurnal land surface heating, are evident for this case in the 3.9-µm band image in Video S1(b). However, it is not possible to approximate near-surface air temperatures in an absolute or quantitative sense based on the infrared window imagery. It is possible, though, to visually distinguish summertime air masses consisting of different temperature and moisture properties during the day, provided approximately consistent land use beneath both air masses, and a proper colour enhancement to provide contrast for small variations in brightness temperature. An expanded discussion of recommended attributes of adequate colour enhancements for operational meteorologists to apply to new-generation satellite imagery can be found in Appendix A.

(2.3) Comparisons

Comparisons with simulated imagery, GOES-13, and surface observations from 30 August 2017 are investigated to determine whether the GOES-16 3.9-µm band imagery is unique in its application.

(2.3.1) Simulated imagery

To corroborate the presence of a front and confirm this particular application of the 3.9-µm band, a radiative transfer model produced simulated GOES "East" contiguous United States imagery for 2200 UTC on 30 August 2017 based on numerical weather prediction (NWP) model output (Greenwald et al., 2016) from a 0000 UTC 30 August 2017 run time. The purpose of this comparison is not to assess the accuracy of the NWP model in resolving the extent and timing of the convection, but instead to compare whether a spatial contrast in brightness temperatures on opposing sides of the front exists in the 3.9-µm band and 10.3-µm band. The simulated imagery confirms that the 3.9-µm band depicts greater brightness temperatures over southern Minnesota and central Wisconsin than the 10.3-µm band, as shown in Figure S2. The orientation of the maximum in the 3.9–10.3 µm band difference shown in Figure S2(c) does not significantly differ from the 10.3–12.3 µm difference (i.e., SWD) shown in Figure S2(d). This is different than the observations for this case, which did not reveal a gradient in 3.9-µm brightness temperatures well south of the front. Though we have no independent observations of the boundary layer composition, aerosol scattering is one likely difference between the actual and simulated imagery for this case. A visual inspection of the simulated 3.9-µm band and 10.3-µm band in Figure S2 reveals a contrast in land surface temperature across the front, indicating a similar contrast in near-surface air temperature.

(2.3.2) GOES-13

The point observations from GOES-13 and GOES-16 imagers in Table S1 show that the 3.9-µm band brightness temperatures for the 30 August 2017 case decrease between 2127 UTC and 2302 UTC on both sides of the front, but the contrast in magnitude between the sites on opposing sides of the front is maintained. The decrease in cloud-free brightness temperatures with time is consistent with the decrease in diurnal heating despite lingering incoming shortwave radiation. Video S1(a) depicts cumulus clouds in the GOES-16 SWD over northeastern Illinois, which decrease in coverage with time, likely due to lessening diurnal heating. Those clouds are less evident in the 3.9-µm band, where brightness temperatures decrease ahead of, and behind, the front in both GOES-13 and -16 imagery with time, as shown in Video S1(b) for GOES-16. GOES-13 does not have a band around 12 µm, precluding the creation and use of a SWD for comparison with GOES-16. While GOES-16 ABI provides additional bands that are helpful in assessing the state of the atmosphere compared to GOES-13, the spectral response functions do not provide the detail of a hyperspectral infrared imager for constructing a profile of the troposphere (Schmit et al., 2009).

(2.3.3) Surface observations

Though a radiosonde sounding is not available to reveal the low-level temperature and moisture profile, as a proxy, the 2-m dew point observation was nearly steady around 18.3 °C at the airport for Rochester, Minnesota, KRST, between 2127 UTC and 2302 UTC 30 August 2017.

This suggests that the aforementioned spectral bands captured cooling land surface temperatures and, in the case of the 3.9-μm band, less reflected solar energy. While 2-m dew points are an appropriate proxy, local effects can influence surface observations that are not otherwise reflected in the larger scale pattern.

Figure S3 depicts the surface observations for select locations, including KRST, relative to brightness temperatures from the 3.9-μm band at 2302 UTC 30 August 2017. There is a gradient in both near-surface temperature and dew point across the frontal zone, indicated by the presence of convective clouds. Gusty winds are out of the northeast where temperatures are lower north of the convective clouds and behind the front. Winds are weaker and generally northwesterly to the south of the front where 2-m temperatures, 2-m dew points, and 3.9-μm band brightness temperatures are greater across southern Minnesota and Iowa. Given that the summer normalized difference vegetation index (NDVI), an indication of land type, does not vary significantly over this area per Robinson et al. (2017), excluding the Great Lakes, inland lakes, and large urban areas, it is possible to ascertain that the contrast in brightness temperature in clear-sky areas is largely due to land surface temperature variations driven by near-surface air temperature, with additional effects from aerosol scattering. A strict relationship between 2-m temperatures, 2-m dew points, and 3.9-μm brightness temperatures is not possible given local or subpixel effects not representative of the surrounding area or the lower troposphere.

(2.4) Colour Enhancements

Given the detail and precision of the data, the value of the GOES-16 imagery for certain applications lies partially in using suitable colour enhancements for visually distinguishing features, phenomena, and, in this case, air masses. Human perception of adjacent shades of isoluminant colours, such as lime green, is limited. Colour enhancements should enable the discrimination of features that have brightness temperatures a few degrees Celsius different.

Figure S4 and Video S1(b), with panels from the Advanced Weather Interactive Processing System (AWIPS) showing the same GOES-16 ABI 3.9-μm band image valid at 2302 UTC 30 August 2017, demonstrate the benefits of a properly configured colour enhancement to the human analyst. Video S1(b) shows a colour-enhanced 3.9-μm band image that aids in clearly distinguishing the post-frontal brightness temperatures in yellow from the greater pre-frontal ones in orange. The colour enhancement used with Video S1(b) also provides contrast between the land surfaces and deep convective cloud, which is cyan, while preserving the intra-feature details. In comparison, Figure S4(a) enhances the pre- and post-frontal brightness temperatures with shades of lime green using a modified colour-value correspondence, making the perception of contrast across the front difficult or impossible without interrogating individual image pixels. Figure S4(b) uses a greyscale enhancement over land, and similarly does not reveal substantial contrast. Adjustments to the brightness temperature range over which the enhancement is applied may enhance details of one feature at the expense of another. Previous limitations to computer hardware and graphics rendering capabilities may have required such steps (d'Entremont and Thomason, 1987). However, when enhancing satellite and other meteorological imagery for modern satellites, this is only necessary in limited circumstances, such as when compositing multiple spectral bands in a fashion that requires reducing the bit depth of each band.

(2.5) Other Cases

In validating these findings related to this extended application of the 3.9-μm band, other summertime cases were examined, including those at night and in different portions of the United States. In general, scenes where the environment supported thunderstorms (e.g., a warm and moist lower troposphere) have similar characteristics to this case when solar illumination is present. However, there are important considerations for analysts seeking to apply this approach as part of a routine operational workflow.

The magnitude of 3.9-µm band brightness temperatures changes diurnally due not only to solar heating of the earth surface that is captured in other infrared window bands, but also solar reflection. This makes different 3.9-µm band images difficult to compare for the purpose of discerning boundaries, fronts, and air masses, except if they are adjacent in time. Even still, there are challenges to overcome. The subsequent cases reaffirm the application as presented in the aforementioned 30 August 2017 case, but also describe potential shortcomings.

(2.5.1) Central Plains, 17 May 2018

The evening of 17 May 2018 provides one such affirming case, as well as a pitfall. Figure S5 shows a boundary between two air masses over eastern Kansas. In the 0.64-µm visible band image in Figure S5(a), the presence of clouds confirms the presence of the boundary, where skies are otherwise clear in its vicinity. In the 3.9-µm shortwave infrared band image in Figure S5(b), this boundary is evident from a gradient in the brightness temperatures. A comparison of 2353 UTC 17 May 2018 surface observations from airport stations in Bartlesville, Oklahoma, KBVO, and Joplin, Missouri, KJLN, support the interpretation of the satellite imagery, particularly the 3.9-µm band image that distinctly shows a contrast between the scene over southwestern Missouri compared to south central Kansas and north central Oklahoma. At Bartlesville, Oklahoma, which is south and west of the gradient, the 2-m temperature was 28.9 °C and the 2-m dew point was 15.0 °C, while at Joplin, Missouri, east of the gradient, the 2-m temperature was 23.3 °C and the 2-m dew point was 17.2 °C. Without the satellite image, such a sharp gradient may not have been apparent; winds were from the northeast at both stations.

To the west of this boundary in Figure S5(b), there are convective clouds and conspicuous minima in 3.9-µm band brightness temperatures immediately to their east. Not all 3.9-µm band brightness temperature gradients correspond to distinct air masses. The solar illumination of the scene must be considered. In western Kansas and western Oklahoma, there are cooler brightness temperatures in the deep convective cloud shadows. There is no evidence these are outflow boundaries; the cooler 3.9-μm band brightness temperatures are mainly the result of lost incoming solar radiation.

(2.5.2) Llano Estacado, 17 May 2018

A similar effect from cloud shadows was noticed in the 3.9-μm band over southeastern New Mexico during the two hours preceding 0002 UTC on 18 May 2018, prior to sunset, as shown in Figure S6. In addition, this case exemplifies swaths of rain-cooled land following the development and passage of thunderstorms, as infrared window bands are useful in assessing soil moisture (Wetzel and Woodward, 1987). The 3.9-μm band brightness temperatures are also decreasing as sunset approaches. Still, accounting for these complications to qualitative image interpretation, the sequence of images depicts a westward-propagating outflow boundary across the arid region of Llano Estacado east of the Sacramento Mountains, evident from cooler 3.9-μm brightness temperatures, and the Guadalupe Mountains near the New Mexico-Texas border.

A nearby surface observation station confirms the passage of the boundary. The 2-m temperature recorded at the airport station for Carlsbad, New Mexico, KCNM, decreased from 37.8 °C at 2253 UTC on 17 May 2018 to 34.4 °C at 2353 UTC, while the 2-m dew point increased from -0.6 °C to 10.0 °C during this same one-hour period. Winds shifted from westerly at the former observation time to southeasterly at the latter, with an accompanying increase in haze and reduction in surface visibility. There was no precipitation reported at or between the observation times at the station.

(2.5.3) Northern Florida, 1 June 2018

While Section 2.5.2 demonstrates the potential application for an outflow boundary, the 3.9-μm band is not always particularly sensitive to subtle variations in the vertical temperature and moisture profile. Figure S7 reveals a common sea breeze example from northern Florida at

1902 UTC on 1 June 2018. In this case, there is no discernable gradient in the Figure S7(b) 3.9-µm band brightness temperatures across the sea breeze boundary, despite evidence of a typical boundary layer evolution along the coastline and inland in the corresponding Figure S7(a) 0.64-µm visible band image, with clear skies and a stable environment south of the inland boundary. An additional similar scenario in the vicinity of Lake Michigan on the same day similarly did not reveal any cross-boundary contrast despite surface observations indicating a marked contrast in air masses.

(2.6) Further Investigation

There are limits to the widespread applicability of using the 3.9-µm band for discerning boundaries, fronts, and air masses. Most notably, no cases over water are investigated here, nor were any winter cases containing snow or ice cover considered. Reflective water and ice-based land surfaces provide significant challenges to this approach. Also, more investigation into nighttime cases is necessary, but the initial assessment of cases suggests a lesser or absent effect, probably due to the loss of Mie scattering of shortwave radiation by aerosols in moist boundary layers. For the discussed 30 August 2017 case, the cross-frontal contrast starting at sunset and during the subsequent overnight was significantly reduced due to radiative cooling. Without solar reflection, the 3.9-µm band may have similar applications to other infrared window bands.

(3) Summary

This case captures a late summertime front over the United States Midwest and illustrates the value of the improvements to the GOES-R ABI for an analyst visually inspecting the imagery to examine the environment, most notably:

- Air surface temperatures alter the sensed land surface temperature in the ABI infrared window bands, presenting evidence of a front. While water vapour cools brightness temperatures in all window bands compared to a dry scene, theory suggests that the 3.9-

μm band is least affected. The 3.9-μm band brightness temperatures from GOES-16 over land surfaces on both sides of the front are greater than from GOES-13 in this case.

- The cloud-free brightness temperatures from the 3.9-μm band are less in cooler and drier air masses than they are in warmer and moister air masses where the land type is similar. Though solar contamination can complicate imagery interpretation during the day, aerosols can elevate cloud-free brightness temperatures to provide cross-frontal contrast.
- The brightness temperatures of the 3.9-μm band will vary based on incoming solar radiation and solar reflection. A SWD can confirm the air mass contrast, especially when attempting to isolate low-level water vapour. The value of the SWD will vary depending on the scene, time of the day, and character of the low-level temperature and moisture profile.
- Other cases confirm this application, though there are potential pitfalls for the analyst as a result of the varying solar illumination of the scene and the depth of certain air masses.

With legacy geostationary imagers, weaker fronts and modest contrast between air masses were not always clearly evident. The ABI infrared band data is precise to less than 0.1 °C for most pixels. With imagery of higher quality than previously available from the geostationary orbit, the ABI provides an opportunity to examine contrast for a far wider range of applications, as this case shows. Future work conducted with the ABI infrared bands should leverage this capability with awareness of the differences when compared to legacy GOES imagers, particularly for the similar infrared window bands. The particular application of leveraging the 3.9-μm band instead of the 12.0-μm band may be particularly useful for imagery from the second satellite in the GOES-R series, GOES-17, where a cooling system failure is leading to noisy longwave infrared imagery around satellite midnight.

Acknowledgments

I am thankful for Timothy Schmit, Mathew Gunshor, and many other colleagues at the University of Wisconsin who have assisted me with their deep on-hand knowledge of geostationary satellites, exploratory posture, and continued willingness to answer many of my inquiries related to satellite imagers and data. I specifically thank Mathew Gunshor for his consultation on, and creation of, Figure S1, and R. Bradley Pierce and Allen Lenzen, who kindly shared their model output used to create Figure S2. National Oceanic and Atmospheric Administration (NOAA) grant NA15NES4320001 for the Cooperative Institute for Meteorological Satellite Studies (CIMSS) supported this work.

Appendix A: Colour Enhancements for Satellite Imagery

Operational meteorologists commonly use false colour, or colour enhanced, meteorological satellite imagery. Compared to previous geostationary satellites, the 3.9-µm band on the ABI has an expanded range to capture both extremely hot and cold pixels for fires and cloud tops, respectively, and with a bit depth of 14, or 16384 incremental values, maintains a sensing precision of less than 0.1 °C at terrestrial temperatures. For this band, an ideal enhancement evenly captures the details of features with a sequence of colours across all temperatures while maintaining sufficient contrast between different features. Due to the number of incremental values, this is challenging, especially since previous satellite imagery and colour enhancements were constrained to a bit depth of eight, or 256 incremental values, which allowed users more variability in colour for adjacent values (sharper colour gradients).

Fairchild (2013) specifies the five characteristics through which humans perceive colour: brightness, colourfulness, hue, lightness, and saturation. However, most images are colorized according to specified red, green, and blue, or RGB, dimensions (Stauffer et al., 2015), commonly because computer and television monitors display output based on such a colour definition model. The challenge for the human analyst viewing an image on a computer or television monitor is that incremental changes in the dimensions of the RGB triplet do not always correspond to the same perceived change to the degree of the colour (Stauffer et al., 2015). For example, shades of lime green, which has a high but constant luminance, are more difficult to distinguish than shades of orange, in which luminance decreases from the yellower shades of orange to redder shades of orange.

References

Ackerman, S.A., 1989. Using the radiative temperature difference at 3.7 and 11 µm to tract dust outbreaks. Remote Sens. Environ. 27, 129–133. https://doi.org/10.1016/0034-4257(89)90012-6

Chesters, D., Uccellini, L.W., Robinson, W.D., 1983. Low-Level Water Vapor Fields from the VISSR Atmospheric Sounder (VAS) “Split Window” Channels. J. Clim. Appl. Meteorol. 22, 725–743. https://doi.org/10.1175/1520-0450(1983)022<0725:LLWVFF>2.0.CO;2

d’Entremont, R.P., Thomason, L.W., 1987. Interpreting Meteorological Satellite Images Using a Color-Composite Technique. Bull. Am. Meteorol. Soc. 68, 762–768. https://doi.org/10.1175/1520-0477(1987)068<0762:IMSIUA>2.0.CO;2

Dostalek, J.F., Weaver, J.F., Purdom, J.F.W., Winston, K.Y., 1997. PICTURE OF THE QUARTER: Nighttime Detection of Low-Level Thunderstorm Outflow Using a GOES Multispectral Image Product. Weather Forecast. 12, 947–950. https://doi.org/10.1175/1520-0434(1997)012<0948:POTQND>2.0.CO;2

Fairchild, M.D., 2013. Color Appearance Terminology, in: Color Appearance Models. John Wiley & Sons, Ltd, Chichester, UK, pp. 85–96. https://doi.org/10.1002/9781118653128.ch4

Gallo, K., Hale, R., Tarpley, D., Yu, Y., 2011. Evaluation of the Relationship between Air and Land Surface Temperature under Clear- and Cloudy-Sky Conditions. J. Appl. Meteorol. Climatol. 50, 767–775. https://doi.org/10.1175/2010JAMC2460.1

Greenwald, T.J., Pierce, R.B., Schaack, T., Otkin, J., Rogal, M., Bah, K., Lenzen, A., Nelson, J., Li, J., Huang, H.-L., 2016. Real-Time Simulation of the GOES-R ABI for User Readiness and Product Evaluation. Bull. Am. Meteorol. Soc. 97, 245–261. https://doi.org/10.1175/BAMS-D-14-00007.1

Hannon, S.E., Strow, L.L., McMillan, W.W., 1996. Atmospheric infrared fast transmittance models: a comparison of two approaches, in: Hays, P.B., Wang, J. (Eds.), . p. 94. https://doi.org/10.1117/12.256106

Kim, Y.J., Sievering, H., Boatman, J.F., 1988. Airborne measurement of atmospheric aerosol particles in the lower troposphere over the central United States. J. Geophys. Res. 93, 12631. https://doi.org/10.1029/JD093iD10p12631

Lindsey, D.T., Grasso, L., Dostalek, J.F., Kerkmann, J., 2014. Use of the GOES-R Split-Window Difference to Diagnose Deepening Low-Level Water Vapor. J. Appl. Meteorol. Climatol. 53, 2005–2016. https://doi.org/10.1175/JAMC-D-14-0010.1

Robinson, N., Allred, B., Jones, M., Moreno, A., Kimball, J., Naugle, D., Erickson, T., Richardson, A., 2017. A Dynamic Landsat Derived Normalized Difference Vegetation Index (NDVI) Product for the Conterminous United States. Remote Sens. 9, 863. https://doi.org/10.3390/rs9080863

Schmit, T.J., Griffith, P., Gunshor, M.M., Daniels, J.M., Goodman, S.J., Lebair, W.J., 2017. A Closer Look at the ABI on the GOES-R Series. Bull. Am. Meteorol. Soc. 98, 681–698. https://doi.org/10.1175/BAMS-D-15-00230.1

Schmit, T.J., Gunshor, M.M., Menzel, W.P., Gurka, J.J., Li, J., Bachmeier, A.S., 2005.

Introducting the Next-Generation Advanced Baseline Imager on GOES-R. Bull. Am. Meteorol. Soc. 86, 1079–1096. https://doi.org/10.1175/BAMS-86-8-1079

Schmit, T.J., Li, J., Ackerman, S.A., Gurka, J.J., 2009. High-Spectral- and High-Temporal-Resolution Infrared Measurements from Geostationary Orbit. J. Atmos. Ocean. Technol. 26, 2273–2292. https://doi.org/10.1175/2009JTECHA1248.1

Stauffer, R., Mayr, G.J., Dabernig, M., Zeileis, A., 2015. Somewhere Over the Rainbow: How to Make Effective Use of Colors in Meteorological Visualizations. Bull. Am. Meteorol. Soc. 96, 203–216. https://doi.org/10.1175/BAMS-D-13-00155.1

Sun, D., 2003. Estimation of land surface temperature from a Geostationary Operational Environmental Satellite (GOES-8). J. Geophys. Res. 108, 4326. https://doi.org/10.1029/2002JD002422

Sun, D., Yu, Y., Fang, L., Liu, Y., 2013. Toward an Operational Land Surface Temperature Algorithm for GOES. J. Appl. Meteorol. Climatol. 52, 1974–1986. https://doi.org/10.1175/JAMC-D-12-0132.1

Wetzel, P.J., Woodward, R.H., 1987. Soil Moisture Estimation Using GOES-VISSR Infrared Data: A Case Study with a Simple Statistical Method. J. Clim. Appl. Meteorol. 26, 107–117. https://doi.org/10.1175/1520-0450(1987)026<0107:SMEUGV>2.0.CO;2

Tables

Table S1 This table compares the Geostationary Operational Environmental Satellite (GOES) brightness temperatures for two locations on opposing sides of a cold front during the evening of 30 August 2017. 2302 UTC is closer to sunset than 2127 UTC over the Upper Midwest of the United States. Rice Lake, WI, was north of the front while Rochester, MN, was south of the front for both times. GOES-13 does not have a band around 12 µm, precluding the creation and use of a "split window" (10.3–12.3 µm) difference (SWD) for comparison with GOES-16. The Advanced Weather Interactive Processing System (AWIPS) was used to compute and collect the data. The locations of Rice Lake, WI, in west central Wisconsin, and Rochester, MN, in southeast Minnesota, can be found on Figure S3 with the station identifiers of KRPD and KRST, respectively.

August 30, 2017	**2127 UTC** ------------- **Rice Lake**	**Rochester**	**2302 UTC** ------------- **Rice Lake**	**Rochester**
GOES-13 3.9-um band brightness temperature	16.5 °C	20.5 °C	14.0 °C	18.0 °C
GOES-16 3.9-um band brightness temperature	20.3 °C	24.4 °C	17.0 °C	21.2 °C
GOES-16 10.3-12.3 um band brightness temperature	3.0 °C	4.8 °C	1.6 °C	3.9 °C

Figures

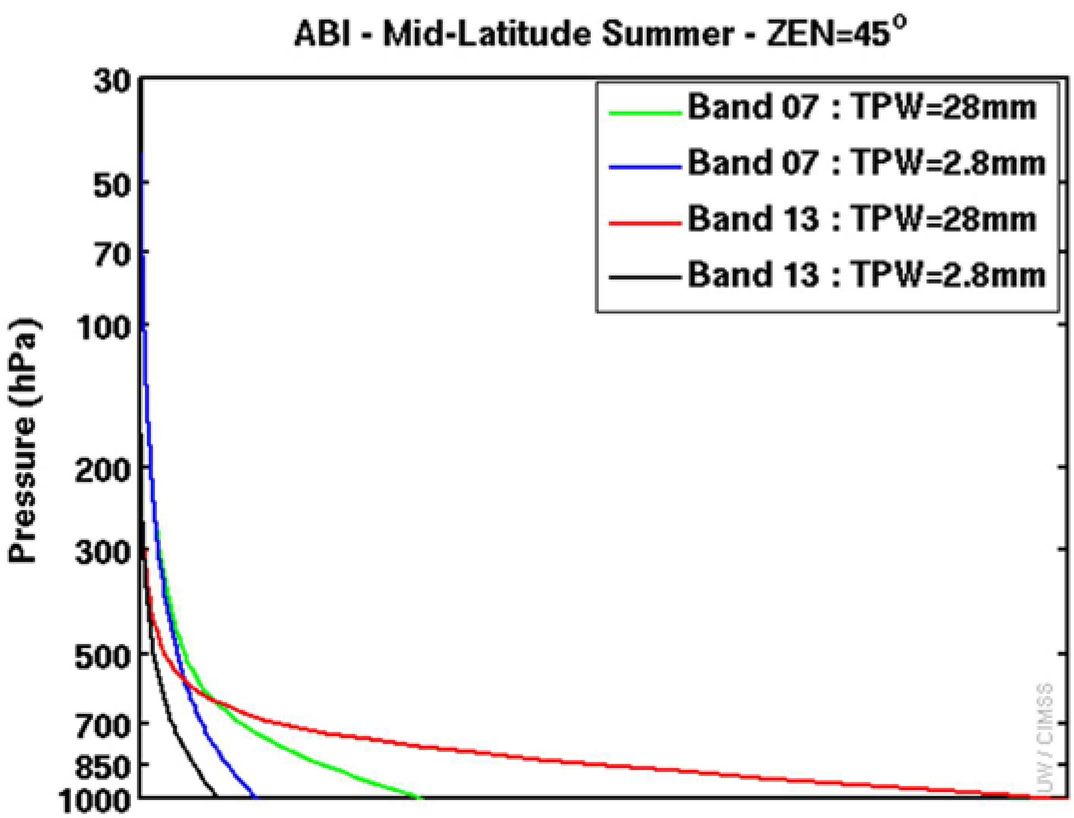

Figure S1 *Window weighting functions.* The four weighting functions calculated according to Hannon et al. (1996) for a cloud-free summertime mid-latitude atmosphere show the influence of low-level water vapor concentration for two window bands on the Geostationary Operational Environmental Satellite 16 (GOES-16) Advanced Baseline Imager (ABI). In moist summertime scenes, the ABI Band 13, the 10.3-µm band, is more sensitive to low-level water vapor than the ABI Band 7, the 3.9-µm band. Compared to the 3.9-µm band, the weighting function profile changes more substantially in the lower troposphere for the 10.3-µm band when the total precipitable water (TPW) decreases from 28 mm, in red, to 2.8 mm, in black, resulting in a simulated 2.0 °C increase in brightness temperature from the moist to dry scene (0.6 °C for the 3.9-µm band). The weighting functions assume a zenith angle of 45°, approximately the angle for GOES-16 ABI viewing of the Upper Midwest from the test position with a subpoint of 89.5° W.

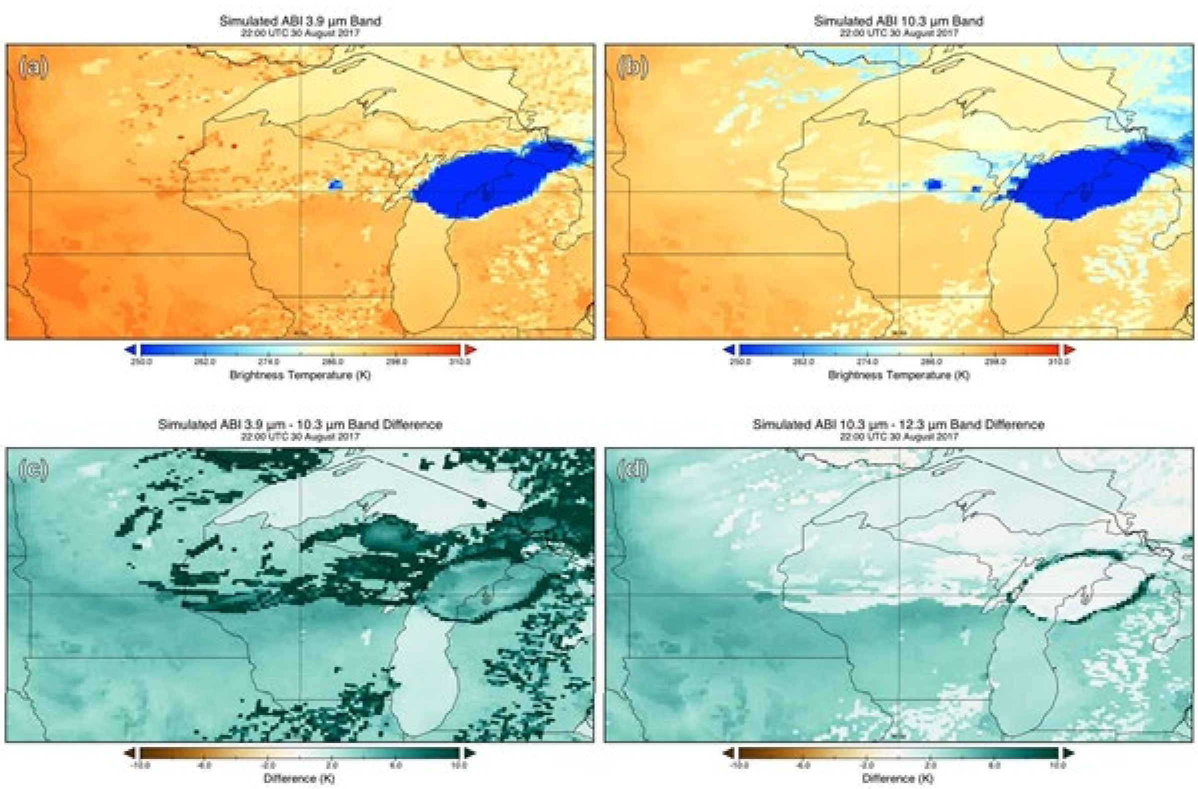

Figure S2 *Simulated Advanced Baseline Imager (ABI) bands and band differences.* This figure depicts the GOES "East", based on a subpoint of 75.0° W, (a) simulated ABI 3.9-µm band, (b) simulated ABI 10.3-µm band, (c) simulated 3.9–10.3-µm band difference, and (d) simulated 10.3–12.3-µm band difference valid at 2200 UTC on 30 August 2017. All four panels contain brightness temperatures in units of Kelvin. Though the convection is underdeveloped over central Wisconsin, the brightness temperatures south of the nearby front are greater than north of it in the top two panels.

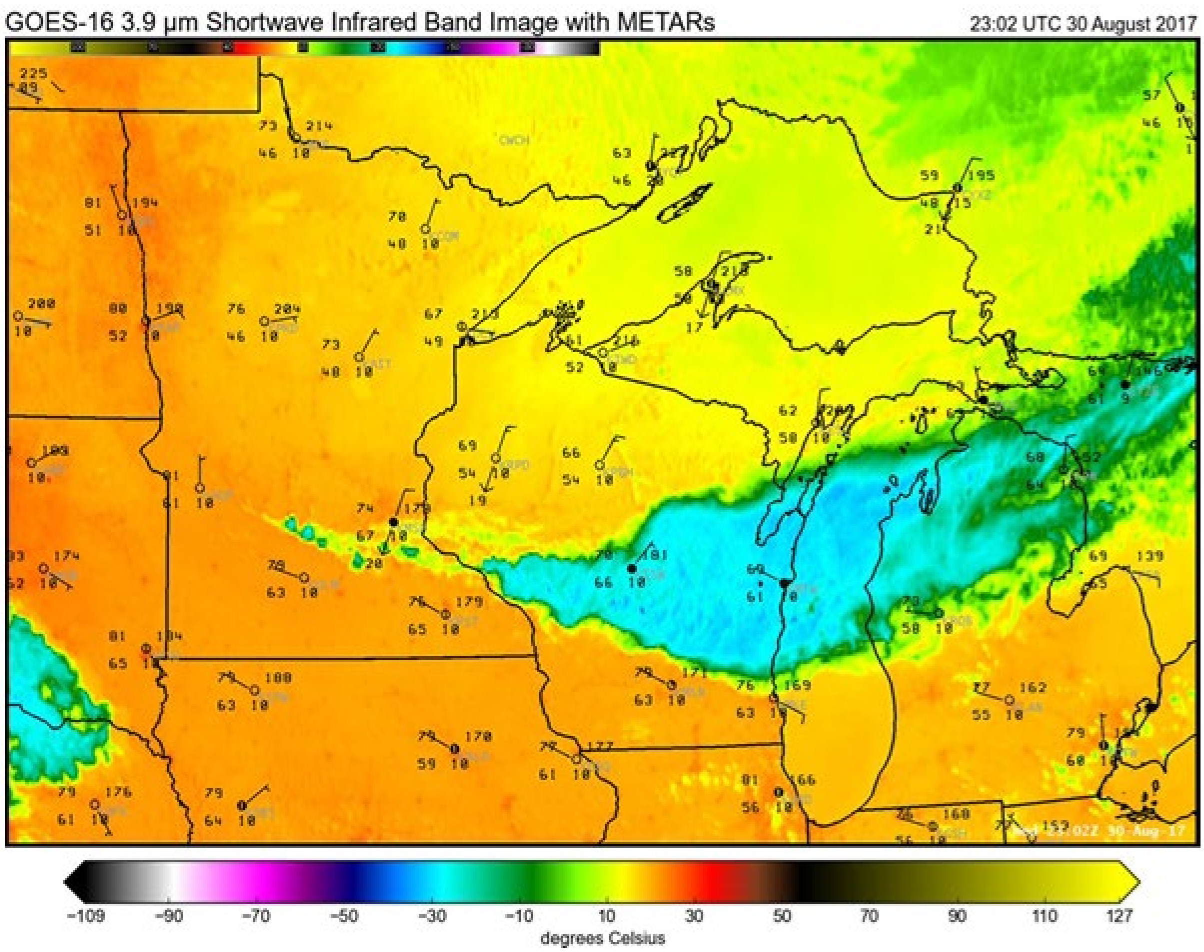

Figure S3 *3.9-µm shortwave infrared band image and surface observations.* This Geostationary Operational Environmental Satellite 16 (GOES-16) Advanced Baseline Imager (ABI) 3.9-µm shortwave infrared band image from the Advanced Weather Interactive Processing System

(AWIPS) is valid at 2302 UTC 30 August 2017. The image also contains plotted Meteorological Terminal Aviation Routine Weather Reports (METARs) in black valid around the same time as the image. Temperatures and dew points are in degrees Fahrenheit. The AWIPS color enhancement applied to the image is “enhanced-rainbow warmer yellow”. The contrast in brightness temperatures to the north and south of the convective cloud is evident with this enhancement.

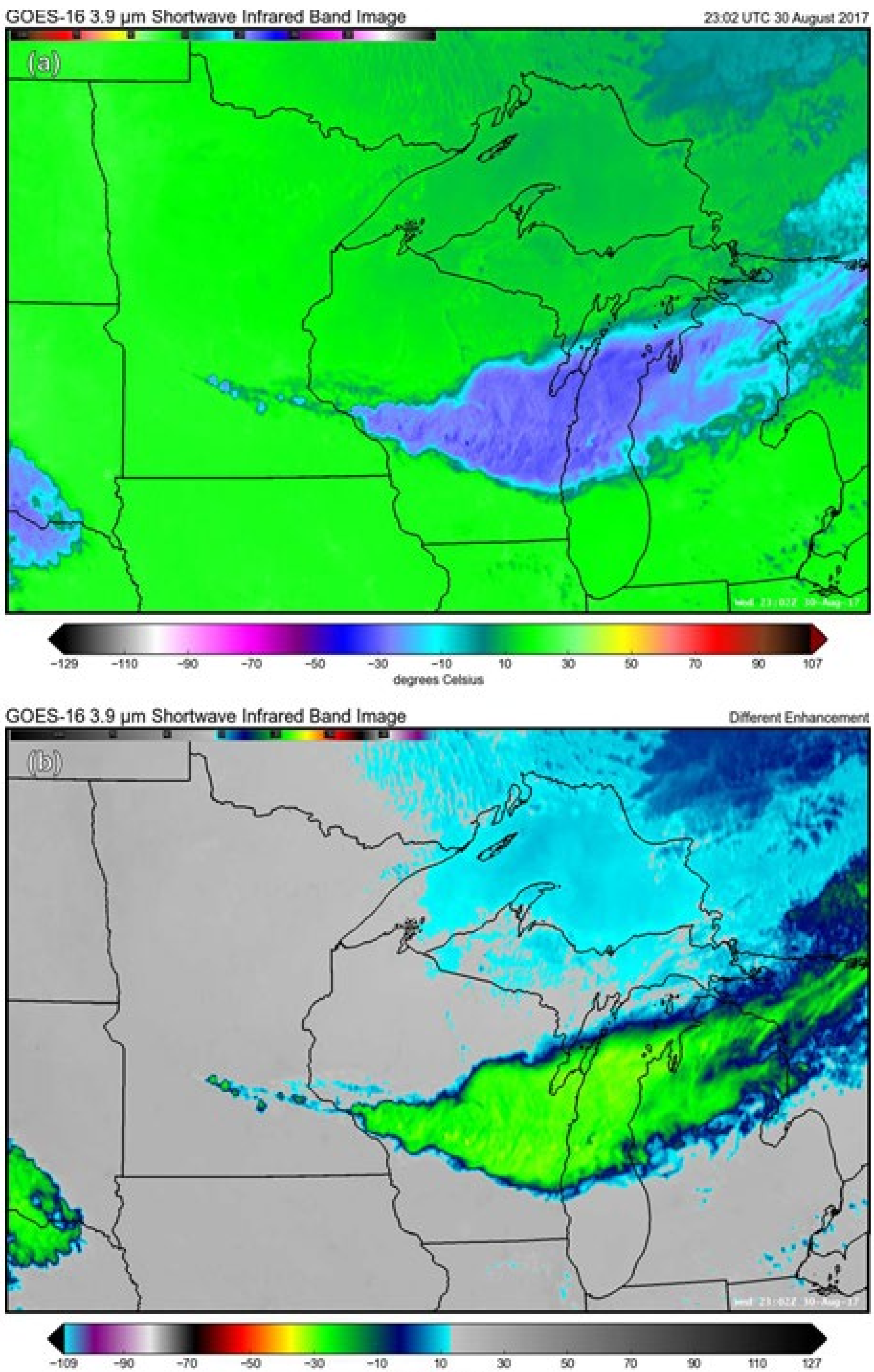

Figure S4 *3.9-µm shortwave infrared band images with different enhancements.* The two panels in this plot contain the same 3.9-µm shortwave infrared band image valid at 2302 UTC 30 August 2017 from the Geostationary Operational Environmental Satellite 16 (GOES-16)

Advanced Baseline Imager (ABI). Each panel has a different color enhancement and color-value correspondence. The Advanced Weather Interactive Processing System (AWIPS) color enhancement applied to the top panel is “Rainbow 11 bit”, and to the bottom panel is “IR Color Clouds Summer”. Neither depicts the contrast in brightness temperatures of cloud-free areas that is evident in Video S1(b).

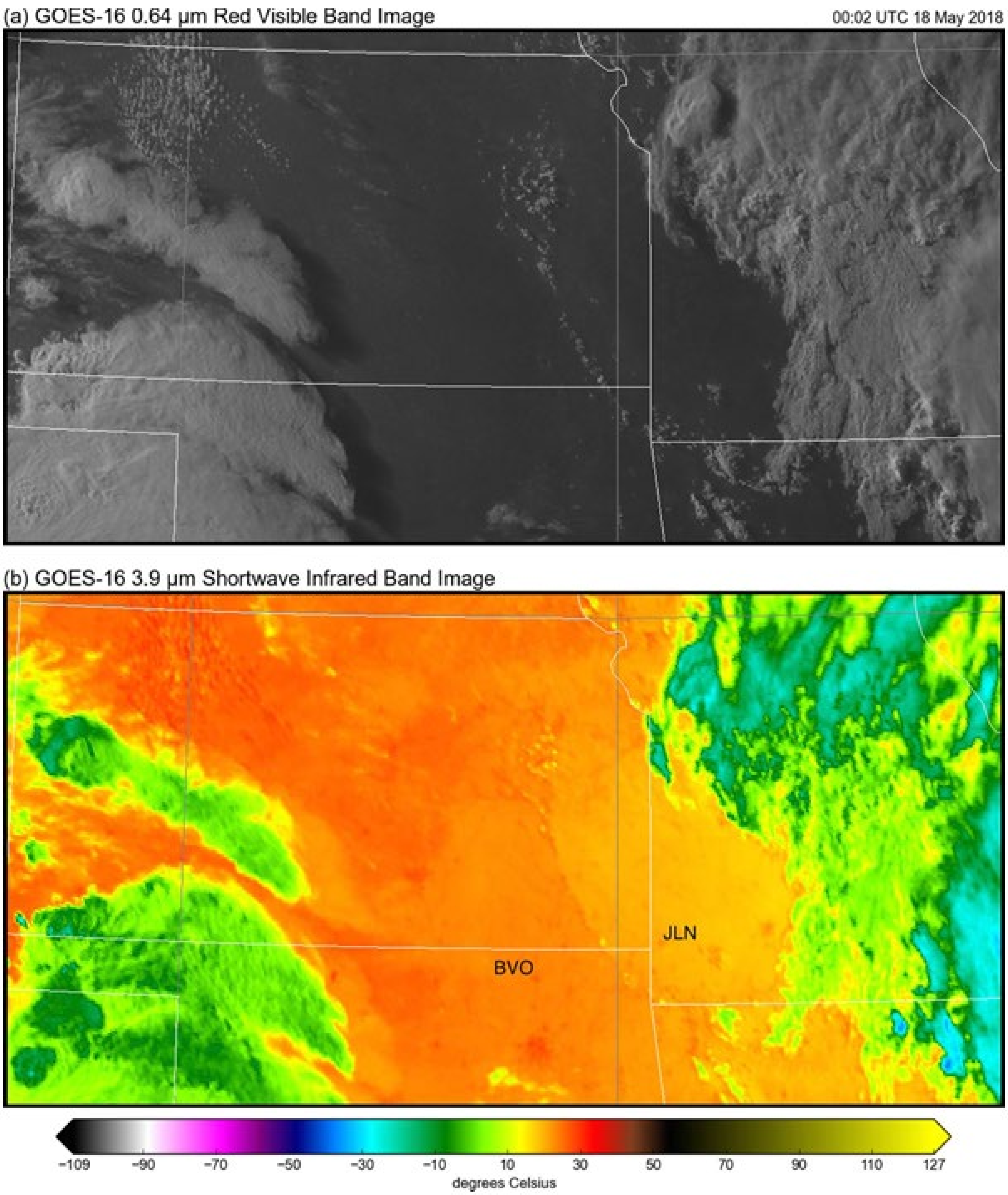

Figure S5 *0.64-µm visible and 3.9-µm shortwave infrared band images of the Central Plains.* The top panel in this plot of Kansas, northern Oklahoma, and Missouri shows the 0.64-µm red visible band image from the Geostationary Operational Environmental Satellite 16 (GOES-16)

Advanced Baseline Imager (ABI) valid at 0002 UTC 18 May 2018, with the corresponding ABI 3.9-µm shortwave infrared band image in the bottom panel. The bottom panel depicts contrasting air masses over western Kansas, where there is a brightness temperature gradient. In addition, the shadow from the clouds evident in the (a) 0.64-µm red visible band over south central Kansas and north central Oklahoma is associated with cooler (b) 3.9-µm band brightness temperatures. The "BVO" and "JLN" labels correspond to the approximate locations of the Bartlesville, Oklahoma, and Joplin, Missouri, weather observation stations, respectively.

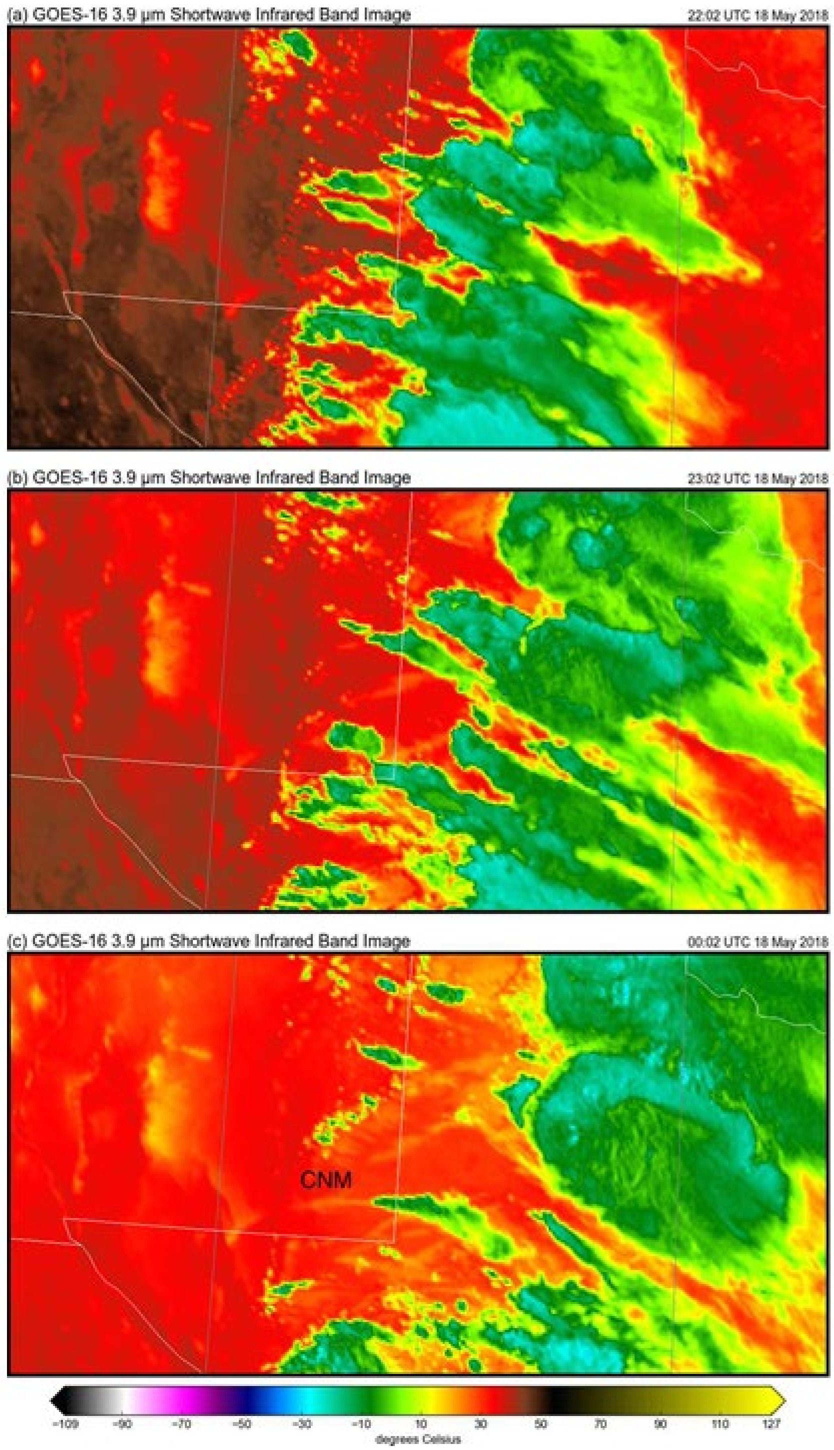

Figure S6 *Time sequence of 3.9-µm shortwave infrared band images of southeastern New Mexico and western Texas.* The three 3.9-µm shortwave infrared band images from the Geostationary Operational Environmental Satellite 16 (GOES-16) Advanced Baseline Imager

(ABI) in this figure depicting southeastern New Mexico and western Texas are valid at (a) 2202 UTC 17 May 2018, (b) 2302 UTC 17 May 2018, and (c) 0002 UTC 18 May 2018, respectively. The panel sequence captures decreasing brightness temperatures as sunset approaches, as well as several swaths of rain-cooled ground from recent thunderstorms. Despite this, differential cooling from westward-propagating outflow over far southeastern New Mexico is evident. The "CNM" label corresponds to the approximate location of the Carlsbad, New Mexico, weather observation station. The Advanced Weather Interactive Processing System (AWIPS) color enhancement applied to the images is "enhanced-rainbow warmer yellow".

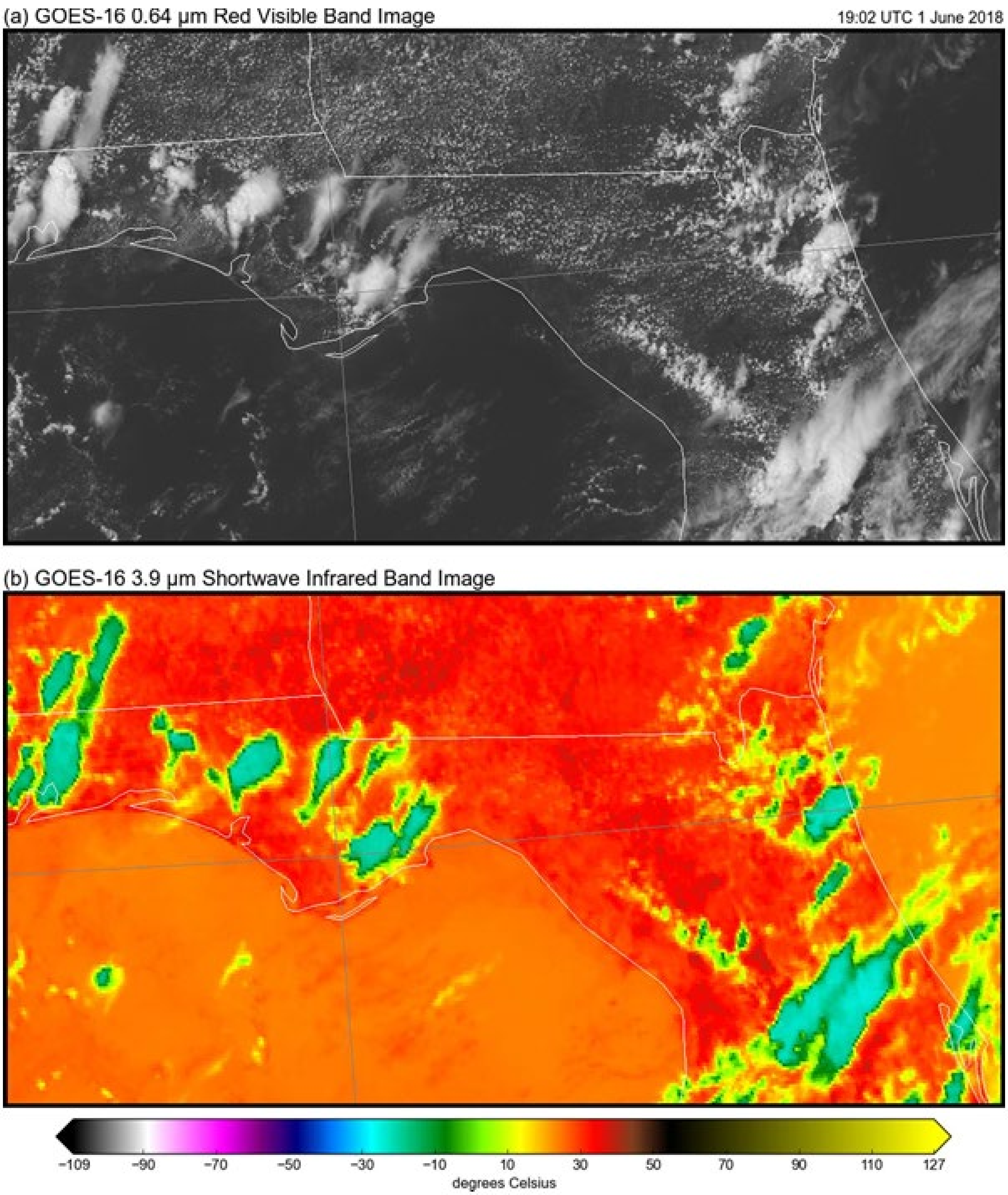

Figure S7 *0.64-µm visible and 3.9-µm shortwave infrared band images of northern Florida.* The top panel in this plot of northern Florida shows the 0.64-µm red visible band image from the Geostationary Operational Environmental Satellite 16 (GOES-16) Advanced Baseline Imager

(ABI) valid at 1902 UTC 1 June 2018, with the corresponding ABI 3.9-µm shortwave infrared band image in the bottom panel. Despite evidence of a well-developed sea breeze in the (a) 0.64-µm reflectances north of the coast, there is no cross-boundary contrast in the (b) 3.9-µm band brightness temperatures.

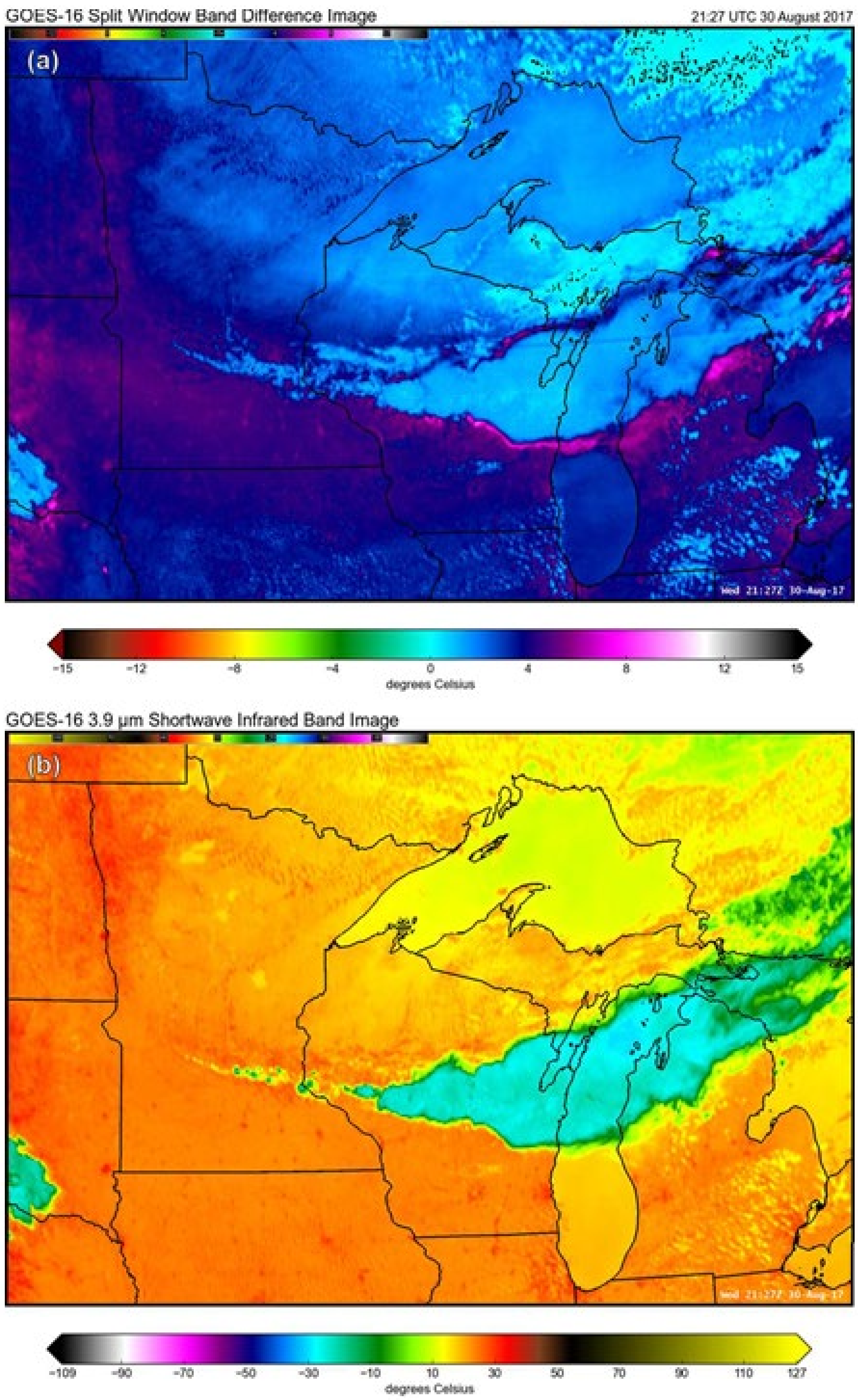

Video S1 *“Split window” (10.3–12.3 µm) difference image with comparison to the 3.9-µm shortwave infrared band image.* This two-panel plot contains a “split window” (10.3–12.3 µm) difference (SWD) from the Geostationary Operational Environmental Satellite 16 (GOES-16)

Advanced Baseline Imager (ABI) in the top panel and the time-corresponding GOES-16 3.9-µm shortwave infrared band image in the bottom panel, both valid at 2127 UTC 30 August 2017. The Advanced Weather Interactive Processing System (AWIPS) color enhancement applied to the top panel is “enhanced-rainbow-11” and to the bottom panel is “enhanced-rainbow warmer yellow”. The brightness temperatures generally decrease in both panels as time progresses and incoming solar radiation subsides, resulting from cooling land surfaces. Black pixels in otherwise cyan areas of the SWD are zero difference values. The animation has images valid every five minutes through 2302 UTC 30 August 2017 (MP4, 2.2 MB).